

# Nonlinear effects in the propagation of optically generated magnetostatic volume mode spin waves

L.J.A. van Tilburg,<sup>1,\*</sup> F.J. Buijnsters,<sup>1</sup> A. Fasolino,<sup>1</sup> T. Rasing,<sup>1</sup> and M.I. Katsnelson<sup>1</sup>

<sup>1</sup>*Radboud University, Institute for Molecules and Materials,  
Heyendaalseweg 135, 6525AJ Nijmegen, The Netherlands*

(Dated: December 3, 2024)

## Abstract

Recent experimental work has shown optical control of spin wave emission by tuning the shape of the optical pulse (Sato et al. *Nature Photonics*, 6, 662 (2012)). We numerically reproduce these results and expand the scope of the control by investigating nonlinear effects. We observe the generation of higher harmonics, leading to short-wavelength excitations and symmetry breaking. In the nonlinear regime we observe self-focusing of the spin waves, as described by the nonlinear Schrödinger equation. These observations open a way for the manipulation of magnetic structures at a smaller scale than the beam focus, for instance in all optical devices.

## I. INTRODUCTION

The study of spin waves, collective excitations of the magnetization, is a subject of great interest in the emerging field of spintronics as they can be used in magnetic switching<sup>1</sup>, manipulation of domain walls<sup>2</sup> and logic devices<sup>3</sup>. One way of generating spin waves in a magnetic system is by means of the inverse Faraday effect (IFE)<sup>4</sup>: a circularly polarized light pulse induces a magnetic field pulse  $\mathbf{H}_{\text{ind}} \propto \mathbf{E} \times \mathbf{E}^*$  where  $\mathbf{E}$  is the electrical component of the incident light. The induced field is directed along the wavevector  $\mathbf{k}$  of the light. The IFE is based on an impulsive Raman scattering process and does not rely on absorption.<sup>5</sup> Thus, the effect can be used to excite spin waves without depositing any heat in the system. Recent experiments by Satoh *et al.*<sup>6</sup> on the garnet  $\text{Gd}_{4/3}\text{Yb}_{2/3}\text{BiFe}_5\text{O}_{12}$  have demonstrated directional control of the spin wave emission pattern. Garnets are specifically suitable for optical spin-wave experiments since many of them have a large magneto-optical response and relatively low spin wave damping.<sup>7</sup> Because nonlinear effects in magnetostatic spin waves have a relatively low exciting threshold<sup>8</sup> and since the magnetization couples so strongly to the optical field, these materials are ideal to study nonlinear effects of the spin wave propagation, such as self-focusing, the concentration of the spin wave power at a single point. This self focusing has to this day only been demonstrated in microstrip experiments, where the spin wave flow was confined along a line.<sup>9,10</sup> We show that by means of the IFE we can excite nonlinear spin waves phenomena in the whole 2D plane and study its evolution spatio-temporally. The tunability and wavemode selection of all optical methods can be used to shape the focal point of the self-focusing spin waves.

## II. METHOD

We are interested in the spin wave pattern that emerges with time when we prepare our system in an initial configuration at  $t = 0$  and calculate the time evolution by integrating the Landau-Lifshitz-Gilbert equation (LLG)<sup>11</sup>

$$\frac{\partial \mathbf{m}}{\partial t} = -\gamma (\mathbf{m} \times \mathbf{H}_{\text{eff}}) + \frac{\alpha}{m} \left( \mathbf{m} \times \frac{\partial \mathbf{m}}{\partial t} \right), \quad (1)$$

where  $\mathbf{m}$  is defined as the magnetization per volume,  $\gamma$  is the gyromagnetic ratio,  $\alpha$  is the Gilbert damping parameter and  $\mathbf{H}_{\text{eff}}$  is the effective magnetic field, calculated as the derivative of the energy with respect to the magnetization.

We consider a uniform slab of thickness  $L$  of a material with out-of-plane easy-axis magnetic anisotropy. We solve Eq. 1 on a  $2400 \times 2000$  square lattice of macrospins with lattice parameter  $a = 1\mu\text{m}$  and periodic boundary conditions.<sup>12</sup> We choose the z-direction normal to the surface. An in-plane static external magnetic field  $H_{\text{ex}}^x$  defines the equilibrium magnetization  $M_S$  along  $\hat{\mathbf{e}}_x$ .

Since the period of the typical spin waves dynamics in our system is much longer than the pulse duration of the incident light, the effect of the optical field can be considered as instantaneous. Thus, in accordance with Eq. 1, for light at normal incidence the IFE leads to a tilt of the magnetization over an angle  $\theta$  in the direction of  $-(\mathbf{m} \times -\hat{\mathbf{e}}_z)$  i.e. the  $-y$ -direction. The profile of the optical pulse determines the spatial extent of the tilted spins. In this paper we consider the tilt angle profiles having the shape

$$\theta(x, y) = \vartheta \exp\left(-\frac{x^2}{2x_0^2} - \frac{y^2}{2y_0^2}\right), \quad (2)$$

where  $x_0$  and  $y_0$  determine the ellipticity of the laser spot. Pulses with  $x_0 \neq y_0$  can be achieved by using an aperture as is done in Ref. 6. The angle  $\vartheta$  modulates the amplitude of the tilt of the excited state. A strong induced field due to the IFE effect would result in a large value for  $\vartheta$ . Since  $|\mathbf{m}|/M_S = 1$ , the local magnetization after the pulse is given by

$$\mathbf{m}(x, y) = \cos(\theta) \hat{\mathbf{e}}_x - \sin(\theta) \hat{\mathbf{e}}_y. \quad (3)$$

Figure 1 shows two excited states as result of the laser pulse for different values of  $\vartheta$ .

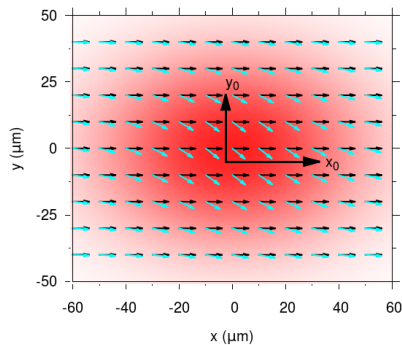


FIG. 1. Two examples of excited states of the in plane magnetization after a pulse with  $x_0 = 35 \mu\text{m}$  and  $y_0 = 25 \mu\text{m}$  and varying laser intensities, according to Eq. 3. The red background shows the intensity profile of the optical field. The small vectors show the magnetization for  $\vartheta = 1^\circ$  (black) and  $\vartheta = 40^\circ$  (light blue).

If we assume a uniform spin wave profile in the z-direction we can calculate the spin wave frequency  $\omega$  of a spin wave with wavevector  $\mathbf{k}$  using<sup>13,14</sup>

$$\omega(\mathbf{k}) = \mu_0|\gamma|\sqrt{\left(H_{\text{ex}}^x + M_S\frac{k_y^2 e^{-kL} + kL - 1}{k^2}\right)\left(\left(H_{\text{ex}}^x + M_S\frac{1 - e^{-kL}}{kL}\right) - \frac{2K}{\mu_0 M_S}\right)}, \quad (4)$$

with  $k^2 = k_x^2 + k_y^2$ , for a system with easy-axis anisotropy  $\mathcal{H}_{\text{ani}} \sim K(\mathbf{m} \cdot \hat{\mathbf{e}}_z)^2$ , an external field  $H_{\text{ex}}^x$  along  $\hat{\mathbf{e}}_x$  and dipole-dipole interactions. For spin waves parallel to the external field  $H_{\text{ex}}^x$  the dispersion reduces to the well known result for volume spin waves in thin films<sup>15</sup>. The exchange length,  $l_{\text{ex}} \propto \sqrt{A/M_S}$  with  $A$  the exchange constant, for garnets is of the order of nanometers<sup>16</sup> and thus very small compared to the resolution of our simulation which is given by the lattice parameter of our spin lattice:  $a = 1\mu\text{m}$ . Therefore, we neglect the contribution of exchange in the following. The uniform mode approximation enables us to simulate the system as effectively two dimensional, greatly decreasing computational costs. Since the lowest order profile of the volume modes is homogeneous throughout the sample<sup>14</sup>, this approximation is also effective beyond the thin-film limit. Figure 2 shows the dispersion of Eq. 4 along the x- and y-axis, using the parameters from table I.

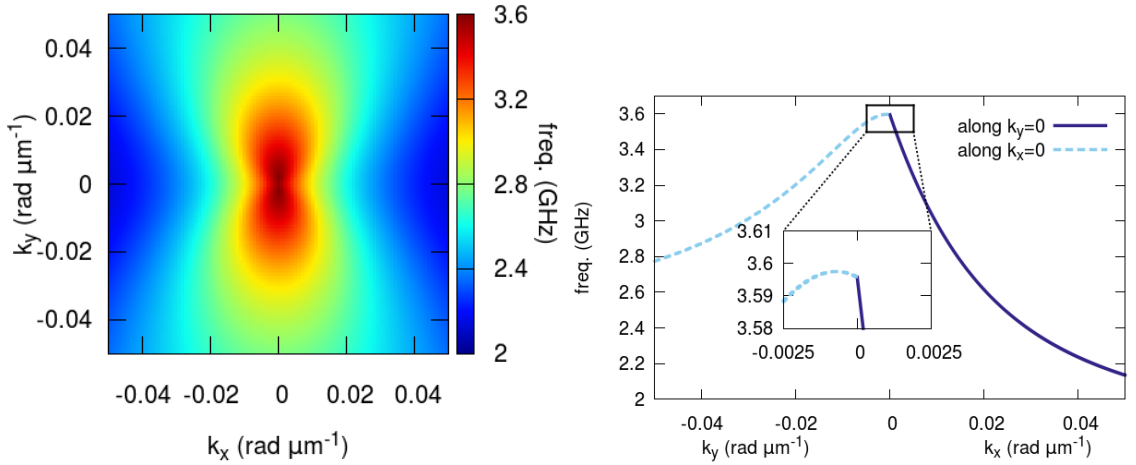


FIG. 2. Left: the dispersion relation for magnetostatic volume mode spin waves in the xy-plane according to Eq. 4. Right: Cut through momentum space along  $k_x$  (solid dark blue line) and  $k_y$  (dashed light blue line). The waves propagating along the external field  $H_{\text{ex}}^x$  all have a negative group velocity. Waves propagating perpendicular to the field have a different behavior for small  $k$ .

The dispersion is anisotropic in the plane because of the external field. For almost all wavevectors  $|\mathbf{k}|$ , the dispersion has negative slope. The associated spin waves are called backward volume magnetostatic waves (BVMSW) due to their negative group velocity. Only for very small values of  $k_y$ , the slope of the dispersion starts out positive, changing sign when  $k_y$  increases. This maximum in the dispersion results from our uniform mode approximation and disappears when the spin wave profile is allowed to vary in the z-direction.<sup>14</sup> In that case, the dispersion starts out flat for small  $k_y$ , decreasing when  $k_y$  increases.

### III. RESULTS

#### A. The linear regime ( $\vartheta = 1^\circ$ )

In this section we make a comparison with the results of Satoh *et al.*<sup>6</sup> where the authors presented experimental results as well as calculations of induced spin wave patterns. However, these calculations were limited to the linear regime ( $\vartheta = 1^\circ$ ) whereas our method is not restricted in its applicability. We show that with Eq. 3 and the parameters listed in table I we reproduce the experimental results of Ref. 6 with the same accuracy. In the next section we will expand the scope to nonlinear effects.

$M_S = 91 \text{ kA/m}$	$\gamma = 1.76 \cdot 10^{11} \text{ rad T}^{-1}\text{s}^{-1}$
$H_{\text{ex}}^x = 99 \text{ kA/m}$	$\alpha = 0.02$
$H_{\text{ani}} = 77 \text{ kA/m}$	$L = 110 \text{ }\mu\text{m}$

TABLE I. Numerical parameters used in the simulations. The value of the anisotropy field is a factor two higher than the experimental value.<sup>6</sup> The need for rescaling of the anisotropy can be attributed to the uniform mode approximation.<sup>14</sup>

Figure 3 shows three snapshots of the spin wave pattern at  $t = 1.5$  ns for the excited state given by Eq. 3 at  $\vartheta = 1^\circ$ . The size and shape of the pump spot is varied using the parameters  $x_0$  and  $y_0$ . The agreement between our calculations and the experimental results presented in Ref. 6 is very good.

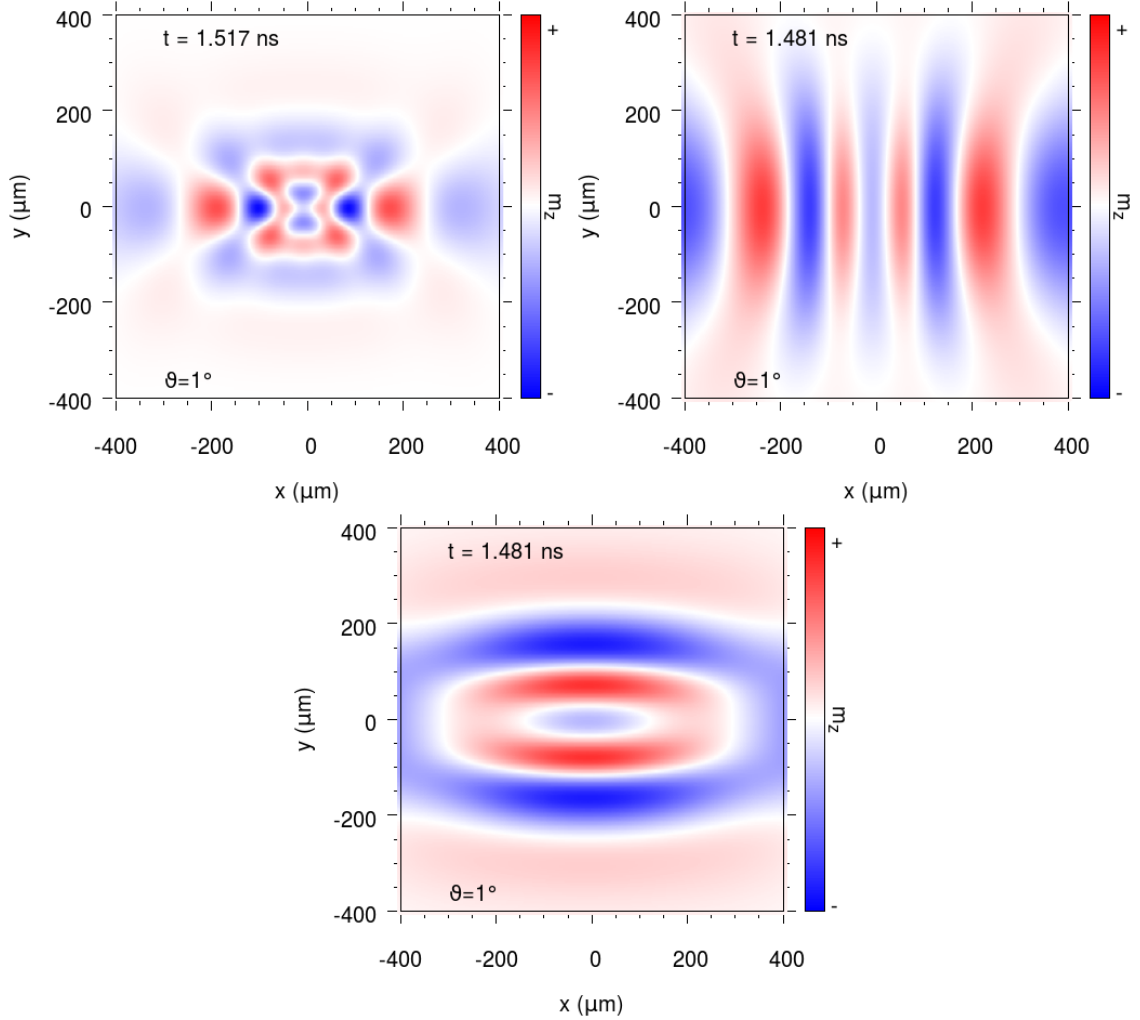


FIG. 3. Three snapshots of the spin wave pattern calculated at  $t = 1.5$  ns. One with a circular initial excitation  $x_0 = y_0 = 25\mu\text{m}$  (top left), and two with an elliptical initial excitation  $x_0 = 35\mu\text{m}$ ,  $y_0 = 140\mu\text{m}$  (top right) and  $x_0 = 140\mu\text{m}$ ,  $y_0 = 35\mu\text{m}$  (bottom). These values have been chosen so that the spin wave patterns can be compared to experimental data in Ref. 6

## B. The nonlinear regime ( $\vartheta > 1^\circ$ )

The amplitude of the tilt of the magnetization in Eq. 3 is given by  $\vartheta$ . For large  $\vartheta$ , we expect to drive the system out of the linear regime. In Fig. 4 we show snapshots of the spin wave pattern at  $t = 1$  ns for six values of  $\vartheta$  and  $x_0 = y_0$ .

We observe a strong dependence on the tilt angle  $\vartheta$ . For increasing values of  $\vartheta$ , features with a small spatial extent become visible near the center of the sample. These short-wavelength modes have a very large amplitude compared to the large-scale features. Furthermore, the symmetry of the spin wave pattern changes. When  $\vartheta = 1^\circ$ , both the  $x$ - and  $y$ -axis are mirror lines for the spin wave pattern but at larger  $\vartheta$ , this symmetry is reduced to a single  $180^\circ$  rotation around the  $z$ -axis.

The appearance of high-intensity small-scale features is also visible in the spin wave pattern with asymmetric pulse shape, ( $x_0 \neq y_0$ ) as can be seen in Fig. 5 when compared with Fig. 3. The shape of the focal point is different in both cases and is determined by the dispersion.

If we study small variations in frequency for a plane wave traveling in the  $x$ -direction on the  $xy$ -plane, we can derive the two dimensional nonlinear Schrödinger equation:<sup>10,15,17,18</sup>

$$i \left( \frac{\partial \varphi}{\partial t} + v_g \frac{\partial \varphi}{\partial x} \right) + \frac{1}{2} \beta_{2\parallel} \frac{\partial^2 \varphi}{\partial x^2} + \beta_{2\perp} \frac{\partial^2 \varphi}{\partial y^2} - N |\varphi|^2 \varphi = 0 \quad (5)$$

following the same notations as in Eq. 4, with  $\varphi$  the dimensionless amplitude of the waves and

$$\begin{aligned} v_g &= \left. \frac{\partial \omega(k_x, 0)}{\partial k_x} \right|_{k=0} && \text{the group velocity,} \\ \beta_{2\parallel} &= \left. \frac{\partial^2 \omega(k_x, 0)}{\partial k_x^2} \right|_{k_y=0} && \text{the dispersion coefficient,} \\ \beta_{2\perp} &= \left. \frac{\partial^2 \omega(k_x, k_y)}{\partial k_k^2} \right|_{k_y=0} && \text{the diffraction coefficient,} \\ \text{and } N &= \left. \frac{\partial \omega}{\partial |\varphi|^2} \right|_{k=0, |\varphi|=0} && \text{the nonlinear coefficient.} \end{aligned}$$

Additional damping of the waves can be included if a term proportional to  $i\alpha\varphi$  is added to the right hand side of Eq. 5. Since it does not qualitatively effect the solutions, we will not consider it in the following.

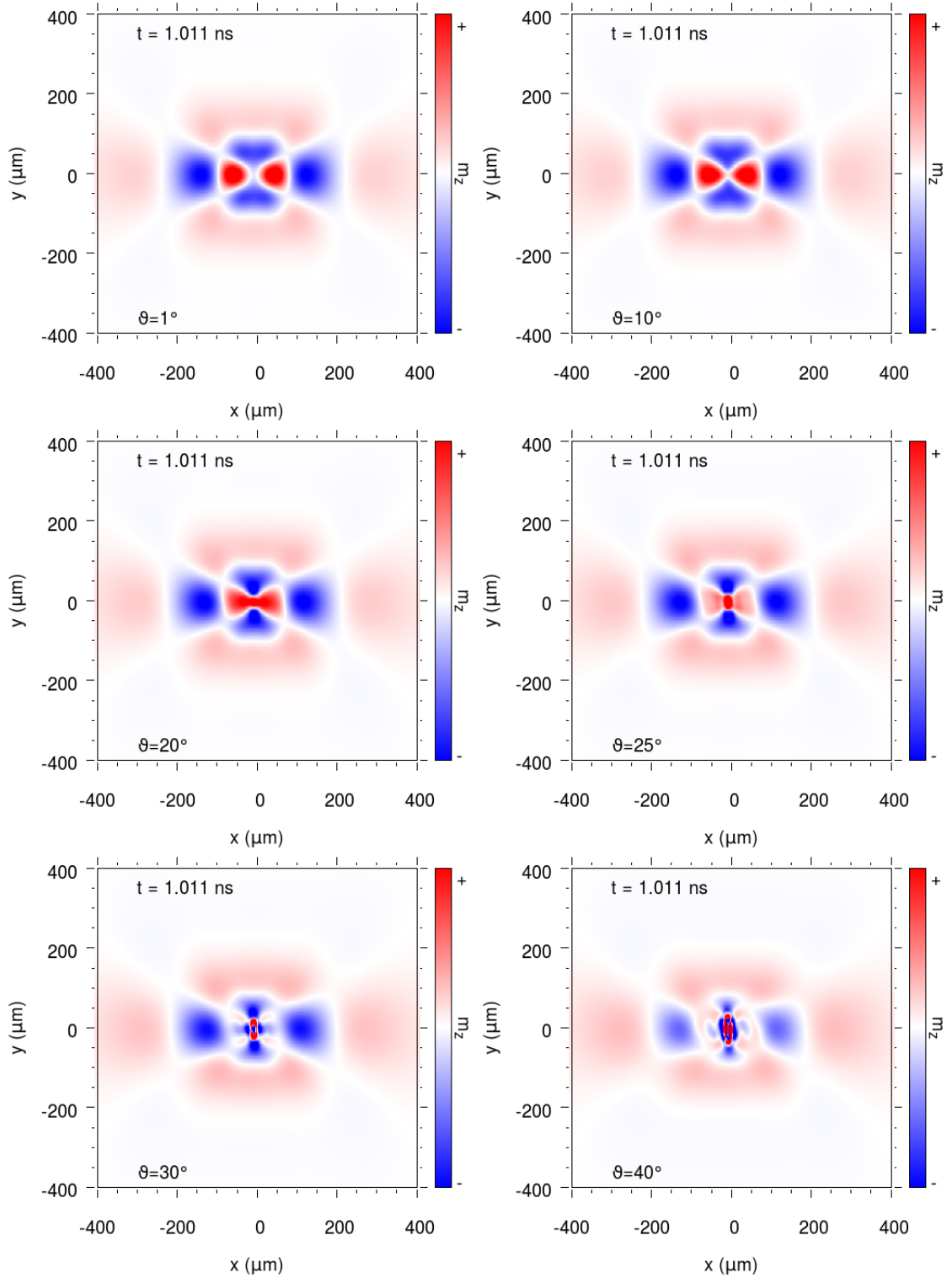


FIG. 4. Six snapshots of the spin wave pattern observed at  $t = 1$  ns with a circular initial excitation  $x_0 = y_0 = |\mathbf{r}_0| = 25\mu\text{m}$  and various values of  $\vartheta$ . From left to right, top to bottom:  $\vartheta = 1^\circ$ ,  $\vartheta = 10^\circ$ ,  $\vartheta = 20^\circ$ ,  $\vartheta = 25^\circ$ ,  $\vartheta = 30^\circ$  and  $\vartheta = 40^\circ$ . The color coding is scaled to the initial amplitude of the tilt  $\vartheta$  to aid comparison between the pictures. For increasing values of  $\vartheta$  the observed spin wave pattern features small wavelength modes near  $\mathbf{g} = 0$ , and the symmetry of the spin wave pattern is broken.

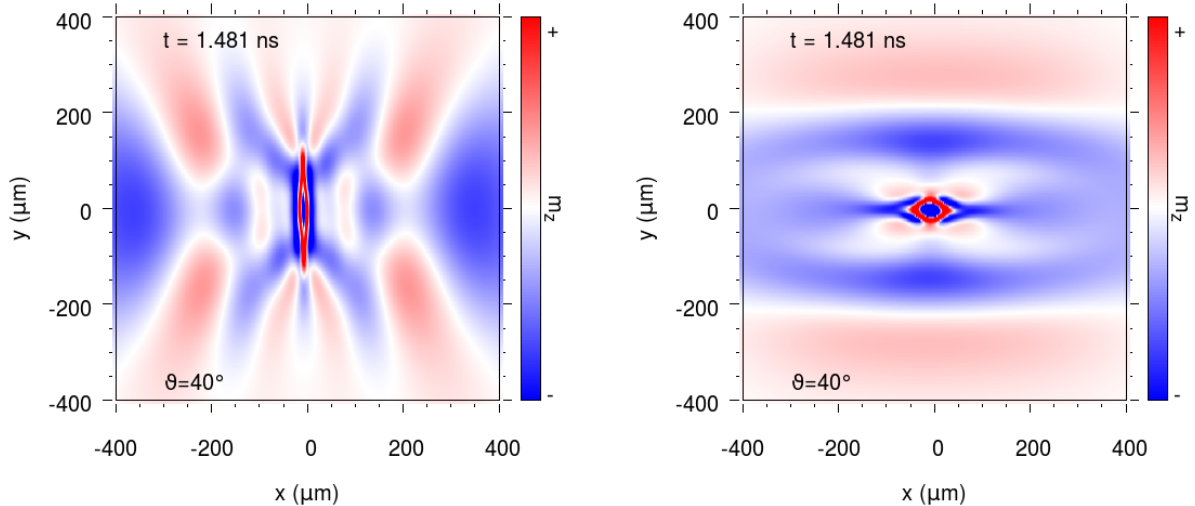


FIG. 5. Two snapshots at  $t = 1.5$  ns of the spin wave pattern for elliptical initial excitations as in Fig. 3 and  $\vartheta = 40^\circ$ . Left:  $x_0 = 35\mu\text{m}$ ,  $y_0 = 140\mu\text{m}$ , right:  $x_0 = 140\mu\text{m}$ ,  $y_0 = 35\mu\text{m}$ . The color coding is scaled to the initial amplitude of the tilt  $\vartheta$  to aid comparison with Fig. 3. For these large values of  $\vartheta$ , the spin waves focus in the center of the beam spot. The spin wave dispersion determines the shape of the focus.

If the dispersion changes when the amplitude of the waves increases, the nonlinear coefficient is nonzero and solutions to Eq. 5 can exhibit self-focusing behavior.<sup>8</sup> This happens when the system becomes unstable to small perturbations and a broad frequency envelope is compressed due to this instability. Since the system also experiences dispersion making the frequency envelope of a wave packet broaden due to different group velocities per wavenumber, these two effects can counterbalance and a stable solitonic solution may be found. This balance between the wave compression and dispersion exist if the system satisfies the Lighthill criterion<sup>17,18</sup>:

$$\beta_{2\perp}N < 0, \quad (6)$$

and these solutions are self-focusing waves.

For both surface and volume magnetostatic waves the sign of  $N$  is always negative.<sup>15</sup> Thus, the sign of  $\beta_{2\perp}$  should be positive to allow for a self-focusing solution to Eq. 5. The second derivative of the dispersion given in Eq. 4 and shown in Fig. 2 is positive for all values of  $\mathbf{k}$ . Note that the maximum in the  $\omega(\mathbf{k})$  near  $k_y \approx 0$  is a consequence of the uniform mode approximation.<sup>14</sup> We conclude that the spin waves can exhibit self-focusing in the 2D plane.

Returning to our numerical results of Fig. 4 and Fig. 5, we see that the self-focusing spin waves are small compared to the dimensions of the focus of the optical pulse. We have observed spin waves with a wavelength of a few  $\mu\text{m}$ , an order of magnitude smaller than the spatial dimensions of the optical pulse. The appearance of the small wavelength modes suggests that for large values of  $\vartheta$ , the system is pushed into the nonlinear regime. For circular excitations the Fourier transform of the excitation is a Gaussian with radius  $|\mathbf{k}_0| = 1/(2\pi|\mathbf{r}_0|)$ . When  $\vartheta$  is small, the distribution of modes in momentum space keeps this Gaussian profile. However, for large values of  $\vartheta$ , modes with  $|\mathbf{k}| > |\mathbf{k}_0|$  become populated. To prove that these higher  $\mathbf{k}$  wavenumbers are the result of higher harmonics generation, we consider the time evolution of a plane wave

$$\mathbf{m}(x, y) = m_0 \hat{\mathbf{e}}_x - \sin(\vartheta) \sin(2\pi\mathbf{r} \cdot \mathbf{k}_{\text{ini}}) \hat{\mathbf{e}}_y, \quad (7)$$

with  $\mathbf{k}_{\text{ini}} = (0.01, 0.005) \mu\text{m}^{-1}$ . In momentum space, this mode gives two sharp peaks at  $\pm\mathbf{k}_{\text{ini}}$ . We find that the distribution in momentum space does not change in time for  $\vartheta = 1^\circ$ . However, when we increase  $\vartheta$  to  $20^\circ$ , modes with integer multiples of  $|\mathbf{k}_{\text{ini}}|$  are present as shown in Fig. 6. Because the initial condition of Eq. 7 is periodic in space and our sample geometry is invariant under rotations around  $\hat{\mathbf{e}}_x$ , there is strong selection for wavenumbers that are odd multiples of  $\mathbf{k}_{\text{ini}}$ . The intensities fit an exponential envelope.

This confirms that for large values of  $\vartheta$ , higher harmonics are generated in the system, which shows that the system is in the nonlinear regime. This is also an explanation for the symmetry breaking that occurs for large values of  $\vartheta$ . The initial excitation of the system, as given by Eq. 3 is symmetric under reflections in the x-axis and y-axis, as is the dispersion. It is therefore not expected that when the system stays in the linear regime, a symmetry breaking can occur. However, since the dispersion is anisotropic, nonlinear effects in the x-direction and the y-direction will differ, breaking the symmetry.

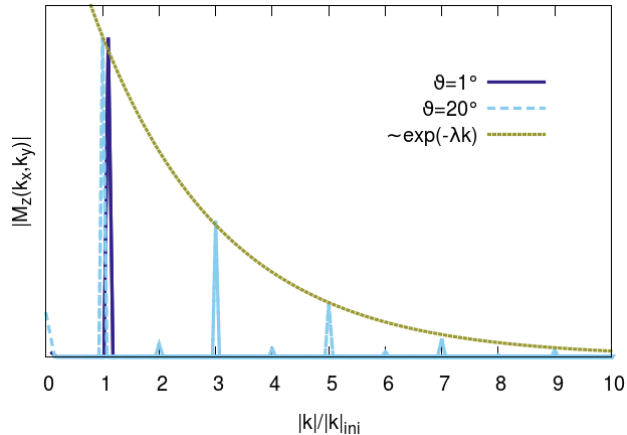


FIG. 6. Amplitude of  $M_z(\mathbf{k})$  along  $\mathbf{k}_{\text{ini}}$  averaged over approximately two full periods of precession for both  $\vartheta = 1^\circ$  (solid dark blue line) and  $\vartheta = 20^\circ$  (dashed light blue line). For easy comparison, we have normalized both spectra to the  $\mathbf{k}_{\text{ini}}$  peak and shifted the data for  $\vartheta = 1^\circ$ . For  $\vartheta = 1^\circ$ , the mode with initial wavevector  $\mathbf{k}_{\text{ini}}$  remains the only mode in the system, whereas at  $\vartheta = 20^\circ$  higher harmonics are clearly visible. Due to the symmetry of the initial condition, odd multiples of the initial wavevector are favored over the even multiples. The harmonics intensities fit an exponential envelope (dotted green line).

#### IV. DISCUSSION

In this paper, we have presented numerical results on volume mode spin wave propagation in  $\text{Gd}_{4/3}\text{Yb}_{2/3}\text{BiFe}_5\text{O}_{12}$ . We modeled the effect of a femtosecond pulse of circularly polarized light by an instantaneous tilt in the saturation magnetization over an angle  $\vartheta$  in the direction perpendicular to the applied field and the equilibrium magnetization. Our simulations were performed in the uniform mode approximation and reproduce experimental results with very good agreement. For large values of  $\vartheta$ , nonlinear effects become clearly visible and small wavelength modes can be seen which are not present in the momentum distribution of the pump pulse. Furthermore, a symmetry breaking of the spin wave pattern can be observed. The small scale modes have a high intensity at the center of the pump spot. Since the second derivative of the dispersion for the BVMSW is positive for any value of the wavenumber, the system can exhibit self-focusing behavior if pushed into the nonlinear regime. Because the system shows the generation of higher harmonics, we are confident that this is the reason why we observe the high-intensity modes at the center of the pump spot.

The shape of the spin wave focus is determined by the spin wave dispersion  $\omega(\mathbf{k})$  and the shape of the incident beam. It is at least an order of magnitude smaller than the focus of the optical pulse.

Our results for small  $\vartheta$  coincide with experimental and computational results in the linear case<sup>6</sup> and predict self-focusing behavior and the generation of higher harmonics for larger  $\vartheta$ . We would like to comment on the experimental feasibility of these large  $\vartheta$ .

A simple calculation shows one requires a magnetic field of  $\sim 0.83$  T for 120 fs to tilt a single spin over an angle of  $1^\circ$ .<sup>19</sup> Thus, it would seem hard to excite large angles in an experiment. However, since the pulse duration is three orders of magnitude shorter than the timescale of the volume mode spin wave dynamics, longer pulses increase the tilt angle without effecting the validity of our approach. Furthermore, since the IFE does not rely on absorption of the incident light, a larger tilt angle could be achieved by increasing the fluence. For instance in the DyFeO<sub>3</sub> garnet a pulse of 200 fs with a fluence of 500 mJ/cm<sup>2</sup> induced fields of 5 T.<sup>4</sup> Additionally, one could also use the direct magnetic component of the pump pulse instead of relying on the IFE. Via the Zeeman term one could push the magnetization out of equilibrium. Reference 20 reported a tilt of  $0.4^\circ$  with a driving field of THz pulses peaking at 0.13 T. Using higher-frequency optical pulses, one can achieve  $\sim 10$  T fields<sup>21</sup>. Thus, we expect that the optically induced nonlinear effects can be experimentally studied.

In the nonlinear regime, the self-focusing leads to large amplitude precession at the center of the pulse spot. The focus of the spin waves is at least an order of magnitude smaller than the dimensions of the provided optical pulse. It would be interesting to perform pump probe experiments in the nonlinear regime and study the self-focusing in the two dimensional plane with both spatial and temporal resolution. Control of the spin wave flow in combination with nonlinear behavior could be useful in technological applications where a strong precession affects the local magnetic structure, such as in switching devices.

## ACKNOWLEDGMENTS

The authors want to acknowledge A. Kimel for his contributions at the start of the project. We want to thank T. Satoh and K. Shen for useful discussions. This work is part of the research program of the Foundation for Fundamental Research on Matter (FOM), which is part of the Netherlands Organization for Scientific Research (NWO). Furthermore, the work is supported by European Research Council (ERC) Advanced Grants No. 338957 FEMTO/NANO and No. 3398BEXCHANGE

---

\* ltilburg@science.ru.nl

- <sup>1</sup> M. Kammerer, M. Weigand, M. Curcic, M. Noske, M. Sproll, A. Vansteenkiste, B. Van Waeyenberge, H. Stoll, G. Woltersdorf, C. H. Back, *et al.*, Nature communications **2**, 279 (2011).
- <sup>2</sup> E. G. Tveten, A. Qaiumzadeh, and A. Brataas, Phys. Rev. Lett. **112**, 147204 (2014).
- <sup>3</sup> R. Hertel, W. Wulfhekel, and J. Kirschner, Physical review letters **93**, 257202 (2004).
- <sup>4</sup> A. Kimel, A. Kirilyuk, P. Usachev, R. Pisarev, A. Balbashov, and T. Rasing, Nature **435**, 655 (2005).
- <sup>5</sup> A. Kirilyuk, A. V. Kimel, and T. Rasing, Reviews of Modern Physics **82**, 2731 (2010).
- <sup>6</sup> T. Satoh, Y. Terui, R. Moriya, B. A. Ivanov, K. Ando, E. Saitoh, T. Shimura, and K. Kuroda, Nature Photonics **6**, 662 (2012).
- <sup>7</sup> F. Hansteen, A. Kimel, A. Kirilyuk, and T. Rasing, Physical Review B **73**, 014421 (2006).
- <sup>8</sup> A. Zvezdin and A. Popkov, Sov. Phys. JETP **2**, 350 (1983).
- <sup>9</sup> M. Bauer, C. Mathieu, S. Demokritov, B. Hillebrands, P. Kolodin, S. Sure, H. Dötsch, V. Grimalsky, Y. Rapoport, and A. Slavin, Physical Review B **56**, R8483 (1997).
- <sup>10</sup> J. Boyle, S. Nikitov, A. Boardman, J. Booth, and K. Booth, Physical Review B **53**, 12173 (1996).
- <sup>11</sup> L. D. Landau and E. M. Lifshitz, Phys. Z. Sowjet. **8**, 153 (1935).
- <sup>12</sup> We are interested in the spin wave propagation in a 2 ns interval. The size of the lattice ensures that the spin waves do not reach the boundaries of the lattice during this interval.
- <sup>13</sup> B. Kalinikos, Microwaves, Optics and Antennas, IEE Proceedings H **127**, 4 (1980).

- <sup>14</sup> F. J. Buijnsters, L. J. A. van Tilburg, A. Fasolino, and M. I. Katsnelson, ArXiv e-prints (2016), arXiv:1602.01362 [cond-mat.mes-hall].
- <sup>15</sup> D. D. Stancil and A. Prabhakar, *Spin waves*, Vol. 1047 (Springer, 2009).
- <sup>16</sup> E. R. Edwards, M. Buchmeier, V. E. Demidov, and S. O. Demokritov, *Journal of Applied Physics* **113**, 103901 (2013).
- <sup>17</sup> G. B. Whitham, *Linear and nonlinear waves*, Vol. 42 (John Wiley & Sons, 2011).
- <sup>18</sup> V. I. Karpman, *Non-Linear Waves in Dispersive Media: International Series of Monographs in Natural Philosophy*, Vol. 71 (Elsevier, 2013).
- <sup>19</sup> J. Stöhr and H. C. Siegmann, *Solid-State Sciences*. Springer, Berlin, Heidelberg , 5 (2006).
- <sup>20</sup> T. Kampfrath, A. Sell, G. Klatt, A. Pashkin, S. Mährlein, T. Dekorsy, M. Wolf, M. Fiebig, A. Leitenstorfer, and R. Huber, *Nature Photonics* **5**, 31 (2011).
- <sup>21</sup> A. Sell, A. Leitenstorfer, and R. Huber, *Optics letters* **33**, 2767 (2008).